Thermoplastic Elastomer Monolayers Grafted to a Functionalized Silicon Surface

Igor Luzinov,† Daungrut Julthongpiput, and Vladimir V. Tsukruk*

Department of Materials Science & Engineering, Iowa State University, Ames, Iowa 50011

Received March 23, 2000; Revised Manuscript Received June 6, 2000

ABSTRACT: We fabricated a robust ultrathin film of a triblock copolymer, poly[styrene-*b*-(ethylene-*co*-butylene)-*b*-styrene] (SEBS), functionalized with 2% of maleic anhydride by melt/solution grafting to a chemically reactive silicon surface. We used epoxy-terminated self-assembling monolayers to functionalize silicon surface. The thickness of grafted block polymer, t, was varied from 1.35 to 9.1 nm to test the limits of stability of microphase-separated structures of the triblock copolymer tethered under confined conditions. Accordingly, the ratio t/d was changed from 0.05 to 0.33, where d is the interdomain spacing. The contact angle measurements demonstrated that the surface of the complete block copolymer films was totally occupied by poly[ethylene-*co*-butene] (PEB) chains. When the SEBS film thickness reached 8.4 nm, the film possessed the well-defined microphase structure of the typical thermoplastic elastomer material, where PS phase formed the microdomain network that reinforced the elastomeric matrix. The microphase separation was completely suppressed only for ultrathin films with $t/d < 0.08$. We found that tethered block copolymer monolayers were extremely stable and preserved their microdomain structure at elevated temperatures unlike physically adsorbed films that dewetted under similar conditions.

Introduction

The block copolymers with immiscible blocks form phase-segregated nanostructures that determine the whole set of their properties.[1] Recently, attention has been drawn to the study of organized thin films from block copolymers, because of their potential for such applications as organized coatings, adhesives, lubricants, and templates for lithography.[2−16] The block copolymers are observed to form microphase morphologies in very thin films. These films undergo a series of structural reorganizations with decreasing film thickness. The surface microdomain morphology depends on the t/d ratio where t is the film thickness and d is the equilibrium spacing of the microdomain structure.[2−4,10,11,13−16] A great deal of the works in this area is devoted to the thin thermoplastic elastomer films composed from ABA block copolymers where A constitutes thermoplastic material (e.g., polystyrene (PS)) and B elastomer (e.g., polybutadiene or ethylene/butylenes copolymer).[6−9] These polymers composed of thermoplastic and elastomeric blocks are called thermoplastic elastomers (TPE). In such materials, the mechanical performance of the reinforced rubber is combined with the straightforward processing of thermoplastics due to the physical network of flexible chains.[1,17]

Van Dijk and van den Berg[6] studied thin films of poly[styrene-*b*-butadiene-*b*-styrene] (SBS) triblock copolymer with the film thickness ranging from 30 to 150 nm. It was found that these films possessed microstructure close to the one for the bulk material, where the PS phase formed a cylindrical microdomain network. The orientation of PS cylinders depended on film thickness. Motomatsu et al.[8] used atomic force microscopy for the investigation of microphase domains of poly[styrene-*b*-(ethylene-*co*-butylene)-*b*-styrene] (SEBS) triblock copolymer film with 170 nm thickness. The surface of the film exhibited characteristic cylindrical morphology typical of the TPE materials with similar composition. In general, to date, the researchers examined relatively thick films ranging from tens to hundreds of nanometers or with the ratio $t/d > 1$.

In this paper, we concentrate on the ultrathin block copolymer layers with $t/d \ll 1$. The purpose of this study is to reveal the morphology and properties of the nanothick triblock copolymer layers as a function of the thickness. In particular, this work is an attempt to answer the question: how thick should the copolymer film be to demonstrate the phase-segregated microstructure typical of triblock copolymers with immiscible blocks? It is necessary to note that scaling down the film thickness to the limit $t/d < 1$ (or to a truly nanometer scale) is a challenging task. Such ultrathin films have a tendency to dewet a surface because of their inherently unstable nature at $t < D$, where D is the size of unperturbed macromolecules.[12]

To avoid the dewetting, we use functionalized triblock copolymer for the tethered film preparation. The functionalized polymer chains tethered to the surface prevent the dewetting.[18,19] We use the triblock copolymer of poly[styrene-*b*-(ethylene-*co*-butylene)-*b*-styrene] functionalized with 2% of maleic anhydride (MA) in the hydrocarbon chains (SEBS) as a TPE material. The epoxysilane self-assembled monolayer (SAM) deposited on a silicon wafer is used as an anchoring interface. We previously demonstrated that the epoxy SAM is homogeneous with terminal epoxy groups mainly located at the SAM surface.[20,21]

Experimental Section

The epoxysilane compound (3-glycidoxypropyl)trimethoxysilane was purchased from Gelest Inc. ACS grade toluene and ethanol were obtained from Aldrich and were used as received. Highly polished single-crystal silicon wafers of {100} orientation (PureSilicon, Inc.) were used as a substrate. The wafers were first cleaned in an ultrasonic bath for 30 min, placed in

* To whom correspondence should be addressed. e-mail: vladimir@iastate.edu.

† Present address: School of Textiles, Fiber and Polymer Science, Clemson University, Clemson, SC 29634.

10.1021/ma000523r CCC: $19.00
Published on Web 09/14/2000

a hot piranha solution (3:1 concentrated sulfuric acid/30% hydrogen peroxide) for 1 h, and then rinsed several times with high-purity water (18 MΩ cm, Nanopure). After rinsing, the substrates were dried under a stream of dry nitrogen, immediately taken into the nitrogen-filled glovebox, and immersed in an epoxysilane solution (1 vol %) for 24 h. After the deposition was complete, modified substrates were removed from solution and rinsed several times with toluene and ethanol. Sample fabrication was conducted under clean-room 100 conditions.

SEBS copolymer was Kraton 1901 (Shell) with styrene and maleic anhydride content 29 wt % and 2 wt %, respectively. The molecular weight measurements were carried out for the SEBS solution in THF using a Waters GPC equipped with Mini Dawn (Wyatt Technology) light scattering detector. GPC data showed $M_n = 41\,000$ g/mol, $M_w/M_n = 1.16$, and $R_g = 6.3$ nm, where R_g is the radius of gyration of SEBS macromolecules. The SEBS copolymer films were deposited on the epoxy-terminated SAM from toluene solution and melt. The MA groups of the rubbery block poly(ethylene-*co*-butylene) (PEB) were able to react with the epoxy groups of the monolayer,[22] thus anchoring the rubber block to the surface.

For grafting from the solution, the modified with epoxysilane silicon wafers were immersed in the copolymer solutions of different concentrations (from 0.25 to 8 wt %) for 24 h. For the grafting from the melt, the initial polymer film was spin-coated from the 1.5 wt % toluene solution onto the wafer modified by the epoxysilane SAM. The thickness of the spin-coated film measured by ellipsometry was 60 ± 6 nm. The specimen was placed in a vacuum oven at 150 °C for 45−360 min to enable the MA groups to diffuse and graft to the epoxy-terminated substrate. In all experiments, the unbounded polymer was removed by multiple washing with toluene, including the washing in an ultrasonic bath. After nine washes, the thickness of the layer did not decrease with additional treatment in an ultrasonic bath. The samples were dried in the covered bottles to provide very slow drying conditions.

Film surfaces were examined by static contact angle (sessile droplet) measurements using a custom-designed optical microscopic system. Droplets (1.5−2 μL) of Nanopure water were placed randomly over the surface. Contact angles were determined within 1 min after the droplet deposition. All reported values were averaged over at least six measurements. The shape of the droplets was observed with a microscope equipped with a CCD camera, and the contact angle was measured at a monitor screen. Ellipsometry was performed with a COMPEL automatic ellipsometer (InOmTech, Inc.) at the angle of incidence of 70°. The silicon oxide thickness was measured for each silicon wafer after the piranha solution treatment and before film deposition. The thickness of the silicon oxide layer was determined to be within 0.8−1.2 nm for different wafers. The index of refraction of the epoxysilane monolayer and silicon oxide was considered to be equal to the "bulk" value.[21] The refractive index for SEBS was estimated via additive molar contributions.[23] All reported thickness values were averaged over six measurements from different parts of the substrate. We used thermal stage form Digital Instrument, Inc., for ellipsometric measurements at elevated temperatures. The temperature change of refractive indexes was estimated via additive molar contributions.[23]

Scanning probe microscopy (SPM) studies were performed in the tapping mode on a Dimension 3000 (Digital Instruments, Inc.) microscope according to the procedure described in detail earlier.[24,25] Silicon cantilevers had spring constants about 50 N/m. Imaging was done at scan rates in the range 1−2 Hz. During the scanning in the tapping mode the cantilever oscillates vertically near its resonance frequency, and the tip makes contact with the sample surface only briefly in each cycle of oscillation.[26] When the tip contacts the surface, the vibrational characteristics of the cantilever vibrations change due to the tip−sample interaction. The feedback mechanism of the tapping mode is controlled by the set-point amplitude ratio $r_{sp} = A_{sp}/A_0$, where A_0 is the amplitude of the free oscillation and A_{sp} is the set-point amplitude such that during scanning the observed amplitude of oscillation is maintained at A_{sp} by adjusting the vertical position of the cantilever.[26] A_0 was chosen about 40 nm. For the "light" and "hard" tapping, the set-point amplitude ratio, r_{sp}, was 0.9 ± 0.05 and 0.45 ± 0.05, respectively, as recommended in ref 7. In absolute terms, it means the whole range for damping of vertical oscillations is 4 ± 2 nm for light tapping and 22 ± 2 nm for hard tapping. For the imaging at elevated temperatures, the thermal stage from Digital Instrument, Inc., that can support predetermined temperature within ±0.2° was used.

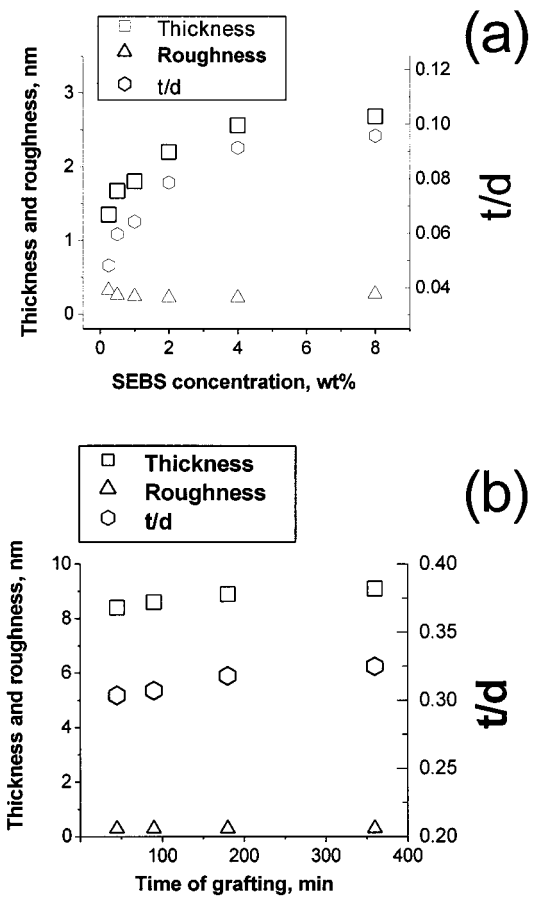

Figure 1. SEBS film thickness as measured by ellipsometry, SPM microroughness, and the film thickness reduced to *d* versus concentration of SEBS in solution (a) and time of the grafting from melt (b).

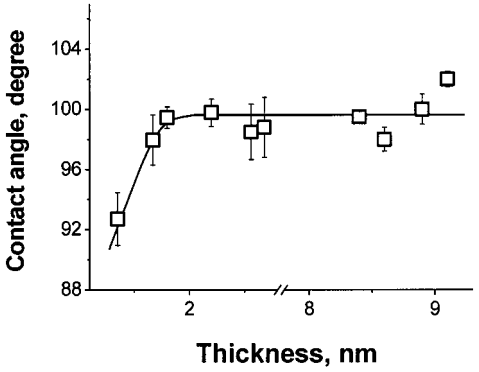

Figure 2. Contact angle for the SEBS monolayers versus the thickness of the film. Line is a guide for the eyes.

Results and Discussion

Thickness and Contact Angle. Figure 1a demonstrates the thickness of SEBS film grafted from solution versus concentration. The layer height gradually in-

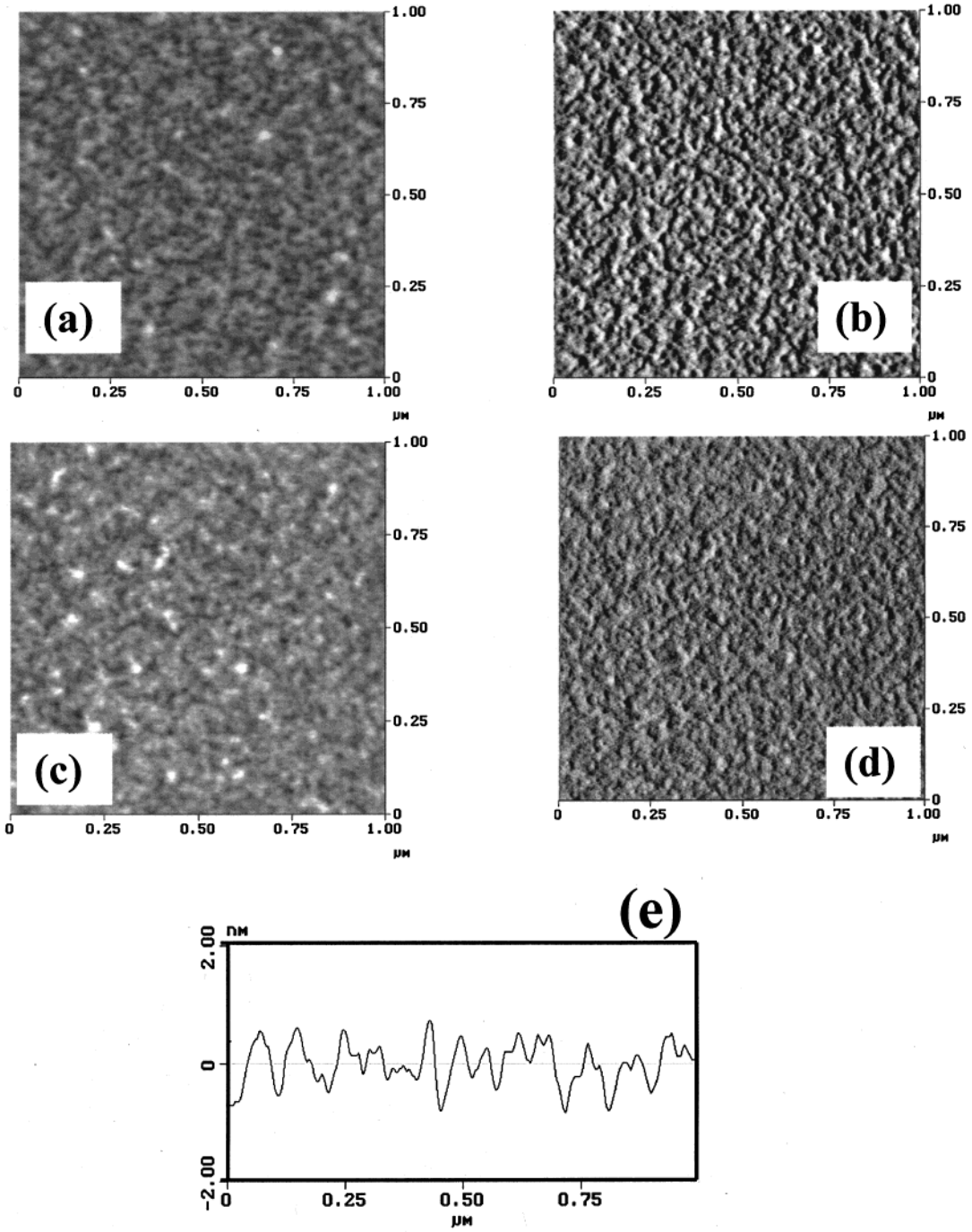

Figure 3. SPM topographical (a and c) and phase (b and d) images of SEBS films with thickness of 1.35 nm ($t/d = 0.05$) (a, b) and 1.8 nm ($t/d = 0.07$) (c, d). (e) Sectional view along the line in the SPM topographical image for the 1.8 nm thick SEBS film. Vertical scale is 7.0 nm and 20° for topography and phase modes, respectively. Bright parts correspond to higher features and phase shifts. "Light" tapping.

creases with the concentration, reaching 2.7 nm at 8%. Grafting from the melt results in much thicker films (8.4−9.1 nm) (Figure 1b). The thickness of the films deposited from the melt depends slightly on the time of the grafting. However, the principal amount of the copolymer (90−95%) is grafted during the first 45 min. Figure 1a,b also presents the thickness of the films scaled with the spacing of microdomain structure, d. For the estimations of the ratio t/d, we use $d = 28$ nm, since this value is reported for a similar SBS block copolymer with very close composition.[27] Indeed, the combination of the grafting from the melt and solution allows us to vary film thickness in a wide range of t/d from 0.05 to 0.33, thus keeping the target condition $t/d \ll 1$.

Figure 2 presents the contact angle variation for the SEBS films. The contact angle varies from 93° for the thinnest film to 100 ± 2° for films with $t > 1.7$ nm. These values are within the range reported for PS surface (90°)[28] and polyethylene surface (99 ± 3°).[29] Since the chemical composition and surface energies of polyethylene and polybutylene are very close,[23] for their copolymer, PEB, we can expect contact angle to be close to 99°. Therefore, the contact angle value indicates that the surface of the block copolymer films is completely occupied by PEB chains except for the thinnest layer. Such a phenomenon, when block with lower surface energy covers the topmost surface, is common for the block copolymer films.[7,15,30,31] The lower contact angle

for films with $t < 1.7$ can be caused by the predominant surface location of PS phase. The presence of PS chains on the surface of the thinnest film can be connected to the fact that the ethylene-*co*-butylene chains are confined due to surface tethering through maleic anhydride groups. When the surface concentration of the grafted polymer is low (as in the case of the thinnest film), the probability that each chain made multiple ties with the substrate is higher. Consequently, the multiple connections may prevent the PEB segments from migration to the air/film interface. For higher film thickness, the fraction of PEB segments (PEB possesses lower surface energy) is located in the topmost layer covering PS blocks.

On the other hand, if SEBS film is adsorbed directly on a bare silicon surface from solution under similar conditions, the contact angle does not reach values for the tethered films. The maximum value that can be reached is only 83°, which is much lower than either contact angle for PS or PEB. This difference indicates that physically adsorbed films are definitely nonuniform with pinholes as was confirmed by microscopic observations (image not shown). The microroughness for these adsorbed film is about 1.2 nm and much higher than the one for the grafted film.

SPM Images Recorded at High Set Point ("Light" Tapping). Figures 3 and 4 present topographical and phase images of the SEBS films with different thickness. The images were recorded using the tapping mode at the highest set-point value (the lowest forces) that permitted a reproducible imaging ($r_{sp} = 0.9 \pm 0.05$,"light" tapping). From the dependence of the amplitude and phase shift on the distance between the sample and the tip (not shown), it reveals that, in this case, we scanned in an attractive interaction regime, and consequently, the topography image reflects the morphology of the topmost layer.[7] At such "light" tapping, the tip−sample interaction is strongly influenced by adhesion attractive forces.[7,32] An attractive force can be considered as a reduction of the effective spring constant of the cantilever−sample system.[33−35] Consequently, the phase of an oscillating cantilever at a fixed drive amplitude is shifted to a lower value. The shift is greater on the surface areas with higher adhesion, because the duration of tip−sample contact is longer for these parts of the surface.

The microroughness of the films measured by SPM under "light" tapping conditions within 1 μm × 1 μm is 0.26 ± 0.04 nm, which is much lower than their thickness (Figures 1 and 2). This observation indicates that the film covers the substrate uniformly without significant holes and bumps as can be seen from cross sections of the topographical image for the grafted films (Figures 3e and 4c). For thin films with the thickness 2.7 nm and lower ($t/d \leq 0.1$), the topographical images show that the copolymer forms densely packed, nanometer-scale clusters distributed homogeneously and completely covering the surface (Figure 3a,c). Figure 4a demonstrates the topography of the film with $t/d \geq 0.3$. This image reveals light surface waviness on a generally smooth film surface. Additionally, small cavities randomly distributed on the surface can be observed. The cavities are 0.4 ±0.1 nm dip.

Under selected scanning conditions ($r_{sp} = 0.9 \pm 0.05$), bright sections correspond to the areas with higher tip−sample adhesion.[37] The thin ($t/d \leq 0.1$) and thick ($t/d \geq 0.3$) films display a very different distribution of

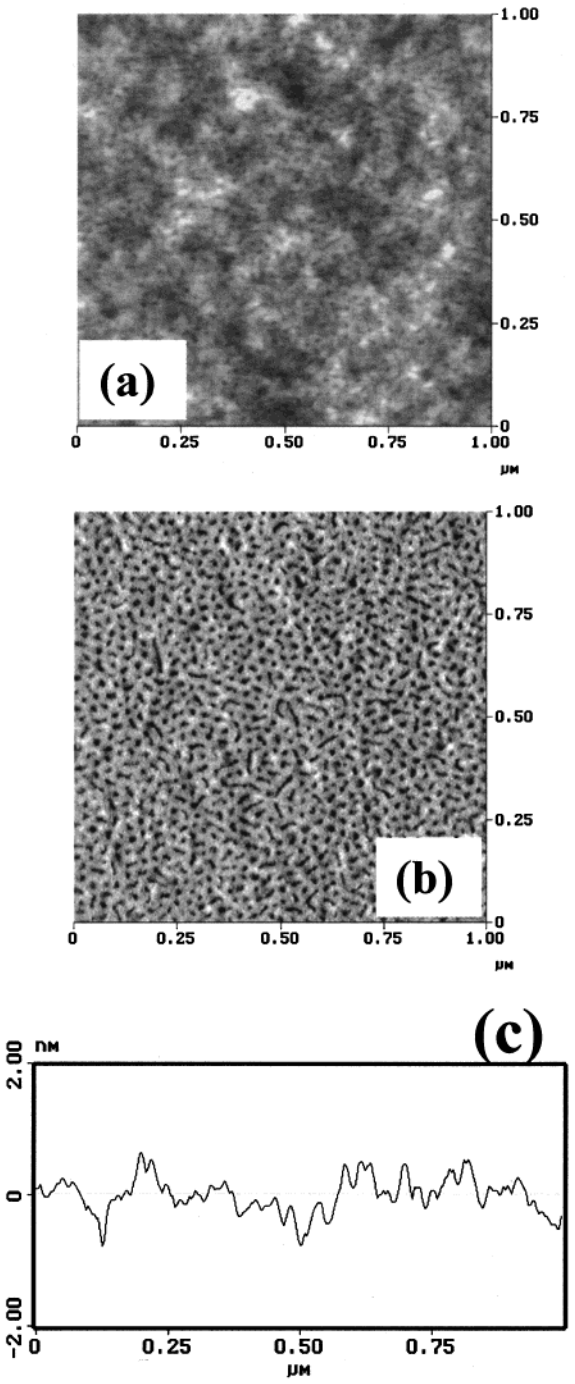

Figure 4. SPM topographical (a) and phase (b) images of SEBS film ($t/d \geq 0.3$) with thickness 8.9 nm. (c) Sectional view along the line in the SPM topographical image for the 8.9 nm thick SEBS film. Vertical scale is 7.0 nm and 20° for topography and phase modes, respectively. Bright parts correspond to higher features and phase shifts. "Light" tapping.

adhesive forces on the surface. For thin films, the surface areas with higher and lower adhesion are randomly distributed (Figure 3b,d). The difference in adhesion between these areas is more pronounced for the thinnest film, where, according to the contact angle measurements, both PS and PEB chains are located on the surface (Figure 2a). Figure 5 shows the root-mean-square deviation (RMSD) of phase shift in image area for the thin samples. For the "light" tapping, RMSD reflects the level of adhesion fluctuation over the film surface. Indeed, RMSD has the highest value for the thinnest film, indicating the highest fluctuation of local

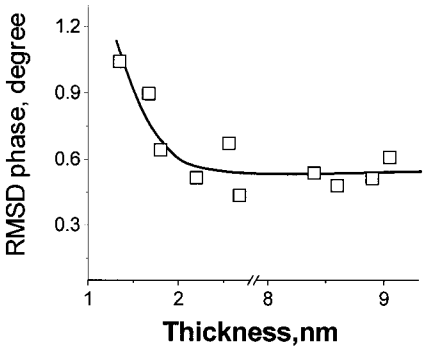

Figure 5. Root-mean-square deviation (RMSD) of phase shift versus the thickness. "Light" tapping. Line is a guide for the eyes.

chemical composition. RMSD practically levels off for $t > 1.7$ nm ($t/d > 0.06$) which reflects more homogeneous surface composition.

For thick films ($t/d \geq 0.3$), the phase image clearly shows the microphase separation typical for the ABA triblock copolymers with immiscible blocks[6−8,27] (Figure 4). Small circular and cylindrical domains with a diameter of 8−12 nm are regularly dispersed in the matrix. Modest widening of the microdomain structure is presented due to the tip contribution, which can be estimated as adding 20−30% of the total width for tips with $R = 5-10$ nm. Therefore, one can estimate the actual lateral dimensions of domains as less than 10 nm. The domains form a pseudohexagonal close packing within the matrix, and the nearest-neighbor distance determined from the 2D Fourier transformation is about 28 ± 2 nm, which is close to interdomain spacing observed for bulk material.[27] It is necessary to note that the location of the tiny cavities on the topographical image corresponds to the position of dark domains on the phase image. In view of the fact that the surface of the film is occupied by PEB chains, the difference in surface adhesion can be connected to the variation in the tip−sample contact area. It is worth noting that more dense areas with higher adhesion should appear brighter on the phase image under the scanning conditions used ($r_{sp} = 0.9 \pm 0.05$).[37] The variation in the adhesion of the topmost layer can be connected with the presence of PS domains located underneath of the PEB layer. Figure 5 displays the RMSD for the thick ($t/d \geq 3$) films versus their thickness. The value of RMSD is rather low and stays practically the same for all "thick" films studied. It reveals that the variation of the tip−sample interaction is very small for different areas.

SPM Images Recorded at Low Set Point ("Hard" Tapping). Figures 6 and 7 present topographical and phase images of the thin and thick SEBS films, respectively. The images were recorded in repulsive mode (r_{sp}

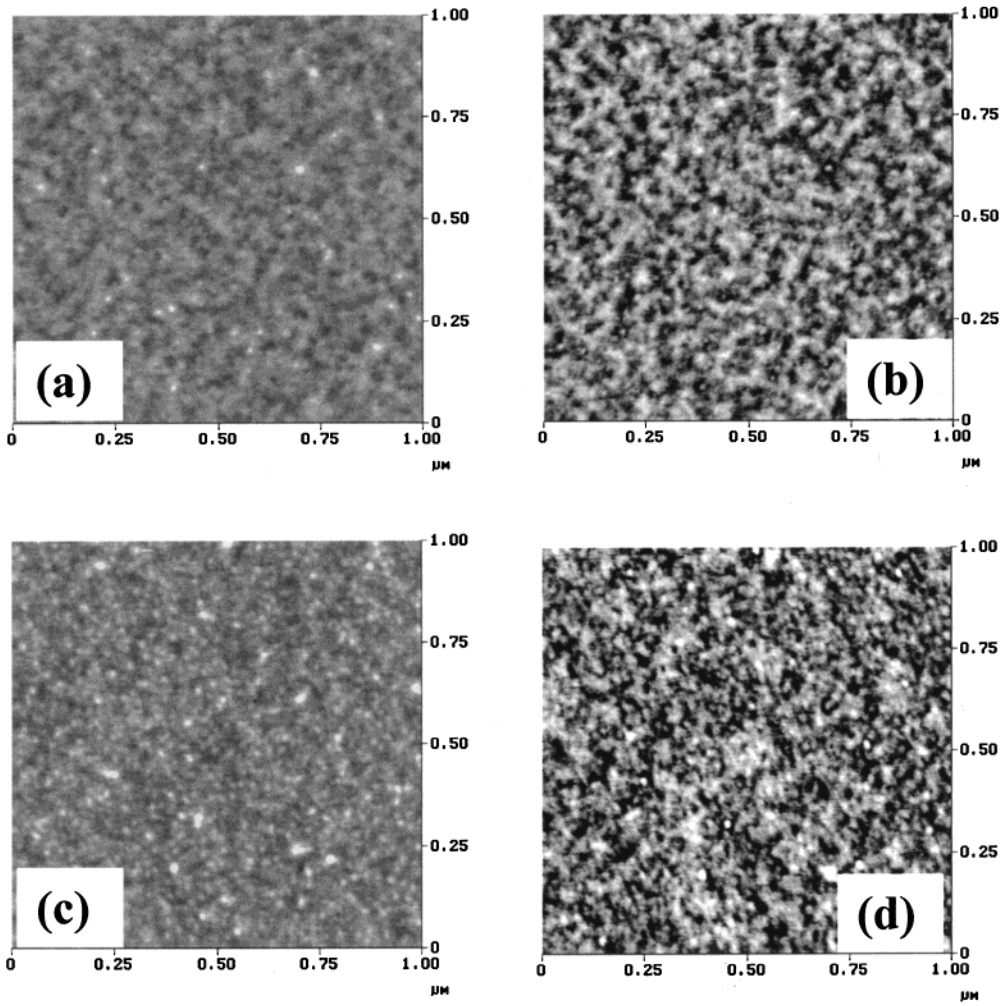

Figure 6. SPM topographical (a and c) and phase (b and d) images of SEBS films with thickness of 1.35 nm ($t/d = 0.5$) (a, b) and 2.6 nm ($t/d = 0.1$) (c, d). Vertical scale is 7.0 nm and 100° for topography and phase modes, respectively. Bright parts correspond to higher features and phase shifts. "Hard" tapping.

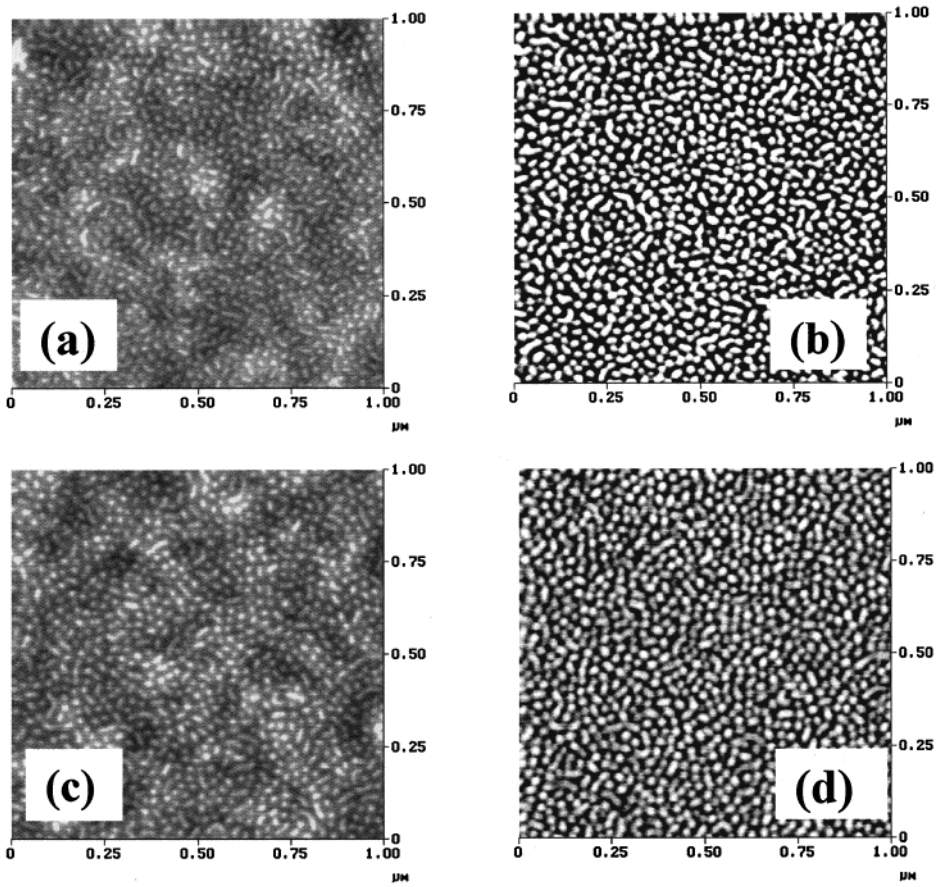

Figure 7. SPM topographical (a and c) and phase (b and d) images of SEBS films ($t/d \geq 0.3$) with thickness of 8.4 nm (a, b) and 9.1 nm (c, d). Vertical scale is 7.0 nm and 100° for topography and phase modes, respectively. Bright parts correspond to higher features and phase shifts. "Hard" tapping.

$= 0.45 \pm 0.05$), as controlled by the dependence of the amplitude and phase shift on the distance between the sample and cantilever. This type of tapping at high forces allows observation of microphase separation that forms underneath the topmost soft polymer layer.[7] The tip squeezes the rubbery part of the film, and hard domains appear brighter in the height image.[7,32,37] For the "hard" tapping the elastic forces due to the deformation of the sample can be described by an additive term to the spring constant of the cantilever−sample system.[33,36] As a consequence of the higher effective spring constant, the resonance frequency increases, which keeps the drive frequency constant, and the phase shift increases. For a soft sample the phase shift is lower than for a stiff sample. Accordingly, hard domains of the block copolymers appear brighter in the phase images.[7,32,37]

Figure 6a,b shows a typical image for thin films. The topographical images are essentially featureless. There is no evidence of the microphase separation typical for the block copolymer materials. When the film thickness increases up to 2.6 nm ($t/d = 0.1$), both topography and phase images display initial stages of microphase separation within the film (Figure 6c,d). The small circular PS domains can be clearly observed.

Figure 8 shows RMSD of phase shift for thinnest films. For the "hard" tapping, RMSD reflects the fluctuation in repulsive forces and indicates the level of elastic heterogeneity within the polymer layer. Generally, RMSD and, consequently, the film heterogeneity are virtually constant for small film thickness. A very low RMSD level indicates the formation of homogeneous polymer layer at this thickness without developed microdomain structure.

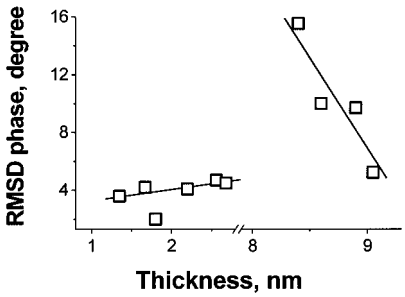

Figure 8. Root-mean-square deviation (RMSD) of phase shift versus the thickness. "Hard" tapping. Lines are guide for the eyes.

Figure 7 shows topographical and phase images for SEBS film with $t/d \geq 0.3$. The microdomain morphology is observed for all samples. The bright circular and cylindrical PS domains are distributed in the dark PEB matrix. For thicker films, the density of the microdomain packing increases (compare parts b and d of Figure 7). The RMSD variation confirms conclusions made from the observation of SPM images. Indeed, for $t > 8$ nm, RMSD rises dramatically, indicating the formation of a highly heterogeneous microstructure (microdomains). With increasing film thickness (and time of the grafting) RMSD decreases gradually (Figure 8). This decrease indicates the formation of a more mechanically homogeneous layer for thicker films.

Figure 9a presents phase image (high forces or "hard" tapping) of spin-coated SEBS film with the thickness of 100 nm ($t/d = 3$). The film is annealed under vacuum at 110 °C for 1 week to reach equilibrium morphology.

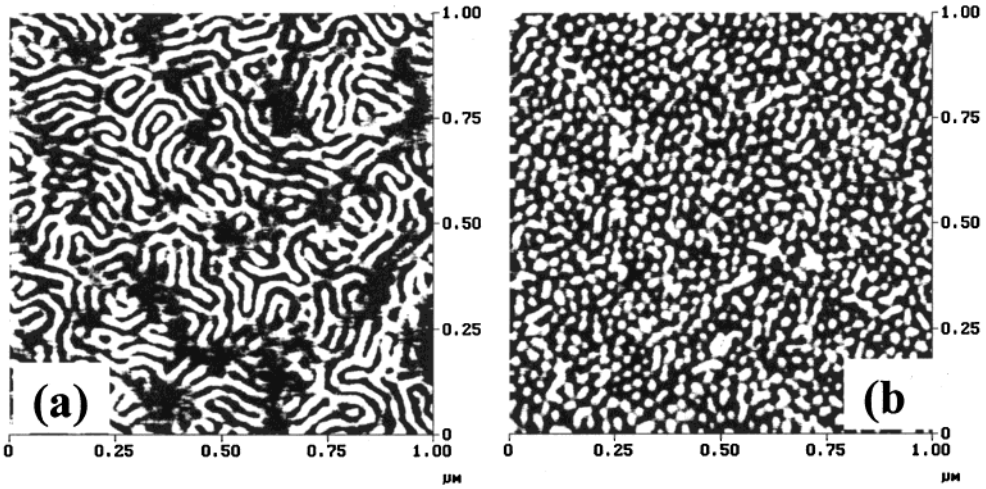

Figure 9. SPM phase images of the annealed SEBS films: (a) spin-coated film 100 nm thick; (b) grafted film 8.4 nm thick. Vertical scale is 20°. Bright parts correspond to higher phase shifts. "Hard" tapping.

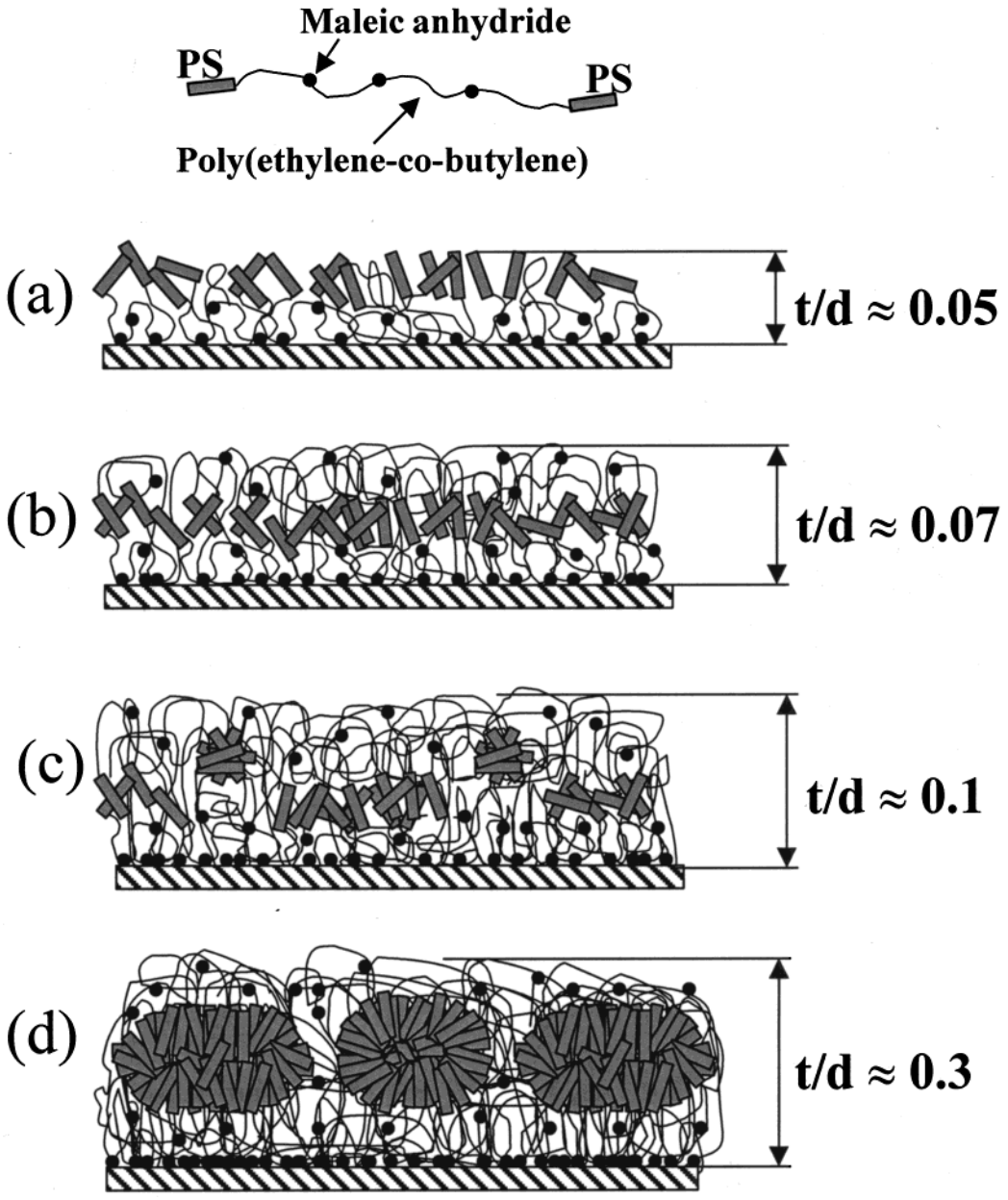

Figure 10. Schematic representation of the SEBS films showing the morphology development at different film thicknesses.

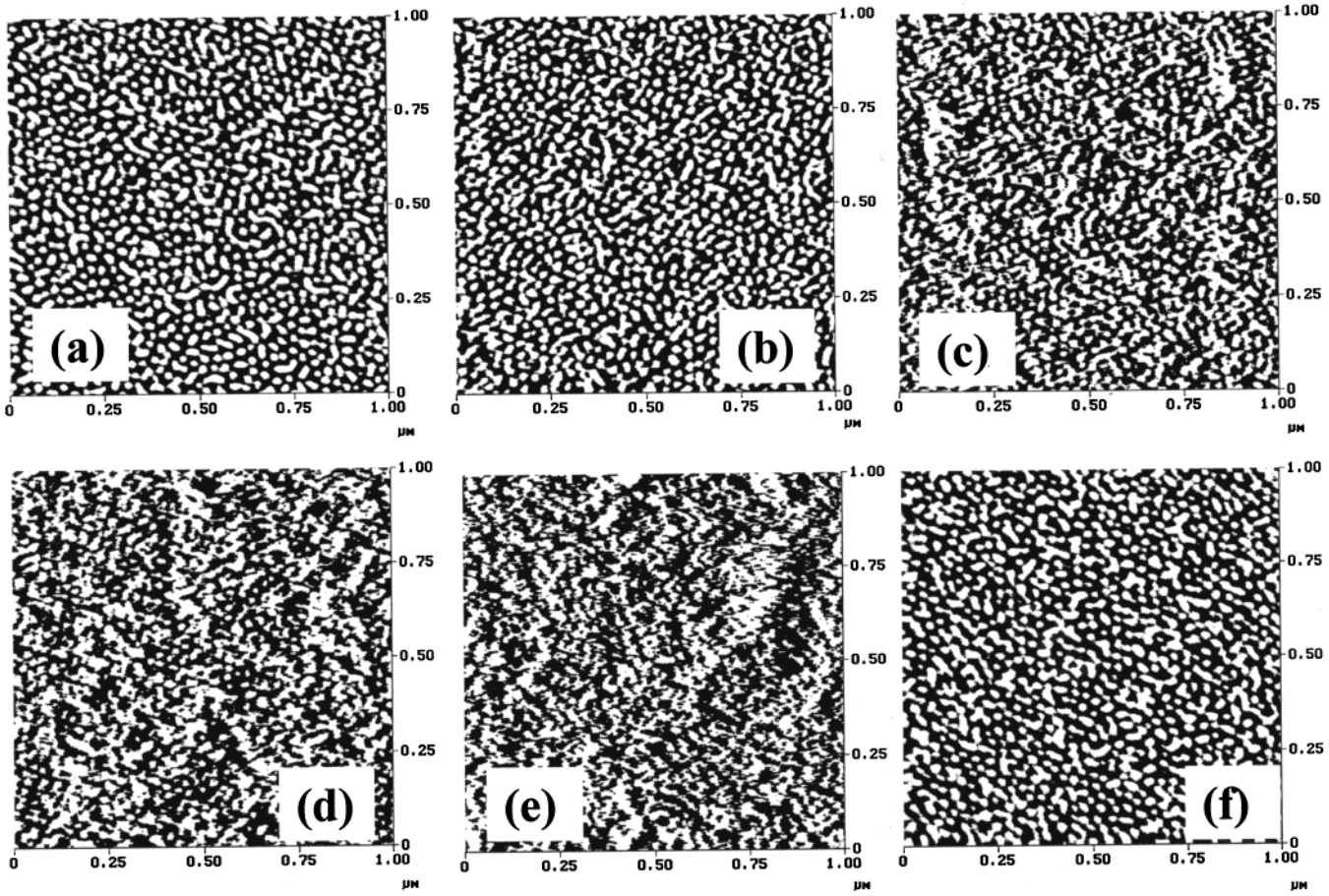

Figure 11. SPM phase images of SEBS grafted film (8.4 nm thick) recorded at different temperatures: (a) 25, (b) 105, (c) 110, (d) 115, and (e) 125 °C. (f) SPM phase image of SEBS grafted film (8.4 nm thick) after thermal treatment at 150 °C for 7 h. Bright parts correspond to higher phase shifts. Vertical scale is 10°. "Hard" tapping.

The phase image shows that the film has cylindrical structure as is anticipated for the bulk SEBS material with the given composition.[8,9] The characteristic spacing of microdomain structure determined from the 2D Fourier transformation is 32 ± 2 nm. This value is slightly higher than the one reported for SBS block copolymers with close composition (d = 27−30 nm).[27]

Figure 9b shows the phase image of the grafted SEBS film (t = 8.4 nm) after the annealing. The microdomain structure of the grafted film after the thermal treatment is virtually unchanged and represents mixture of circular and cylindrical domains unlike thick SEBS film (compare parts a and b of Figure 9). Apparently, in thin film, the chemical grafting of rubber block to surface prevents the formation of well-developed cylindrical structure with microdomain spacing much larger than film thickness.

Morphology Development in SEBS Monolayers. Here, we summarize our observations of SEBS film microstructures. We observe several different morphologies of the grafted SEBS monolayer with different thicknesses. When the grafted film has thickness of 1.35 nm (t/d = 0.05), rubbery blocks of SEBS are predominantly located close to the substrate surface, and the topmost layer is mostly occupied by PS chains (Figure 10a). As the thickness reaches 1.8 nm (t/d = 0.07), the uppermost layer consists mainly of PEB chains (Figure 10b). PS chains are distributed randomly within the SEBS layer.

For the film 2.6 nm thick (t/d = 0.1), the first evidence of the microphase separation within SEBS film is detected. We observe circular PS domains covered by PEB layer as shown in Figure 10c. When the SEBS film reaches t = 8.4 nm (t/d = 0.3), the film displays the microsegregated structure. The PS phase forms the microdomain network cross-linking the elastomeric matrix (Figure 10d). The array of circular and cylindrical PS domains is distributed in the PEB matrix tethered to epoxy-terminated SAM. The PS microdomains have shapes of compressed spheres and cylinders.

Thermal Properties of Grafted SEBS Monolayers. The fundamental property of the thermoplastic elastomer materials is their ability to form thermally reversible cross-linking by glassy domains.[1,17] The material behaves as vulcanized rubber in many respects, while the domains soften when heated above the PS glass transition temperature, T_g. We investigate the structure of the grafted SEBS film of 8.4 nm thickness from the room temperature to 125 °C. From DSC measurements, we detected T_g of the PS blocks in bulk SEBS to be about 75 °C, which is close to T_g observed for bulk PS with a similar molecular weight.[38]

Figure 11b presents the microstructure of the SEBS film at 105 °C. The phase image shows PS microdomains at this temperature identical to the microstructure at room temperature (Figure 11a,b). At 110 °C, PS microdomains can be still detected by SPM; however, the edges of the domains become fuzzy (Figure 11c). When the temperature reaches 115 °C, only isolated domains can be found (Figure 11d). Figure 11e shows that at 125 °C the PS microdomains are not

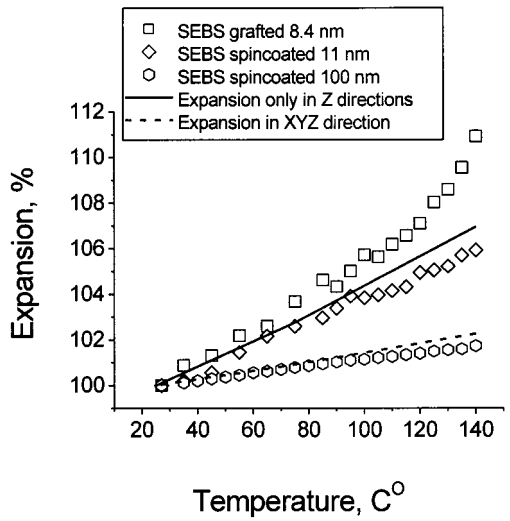

Figure 12. Thermal expansion of the thickness of various SEBS films.

detected, and the film looks completely homogeneous. Observed changes are completely reversible (Figure 11f). Obtained results reveal that at the temperature well above T_g the PS chains are still segregated into a microdomain structure within the grafted film. The microdomains become undetectable only when the temperature of the film reaches a temperature close to the temperature of the order−disorder transition measured for a similar triblock copolymer.[39]

We measured the thermal expansion of the grafted SEBS film (t = 8.4 nm) by monitoring the temperature variation of the film thickness by ellipsometry. We conducted the comparative measurements for thin (11 nm) and thick (100 nm) spin-coated SEBS films as well (Figure 12). For the thermal expansion of the films, two limits can be identified. The expansion in all three possible directions (*XYZ* expansion) is possible for the unrestricted film. When macromolecules are attached to the surface, the expansion in *X* and *Y* directions (in plane) is restricted. Therefore, the film can expand only in the vertical direction (*Z* expansion). Solid and dashed lines in Figure 12 correspond to thickness variation in these two cases. These plots are calculated from the temperature dependence of the SEBS density, which was estimated via additive molar contributions.[23] Excellent agreement is observed between experimental data for the film of 100 nm thick and *XYZ* expansion (Figure 12). This behavior is anticipated, since the majority of chains of the thick polymer film is not in contact with the surface and, consequently, has no limitations for their expansion in *Y* and *X* directions.

The chemically grafted film expands only in the vertical direction, as clearly seen in Figure 12. However, the observed expansion is somewhat higher than the calculated one from the dependence of SEBS density on temperature. The rate of thermal expansion of the thin spin-coated film (11 nm) lies between those for the grafted and thick (100 nm) films. Taking into account

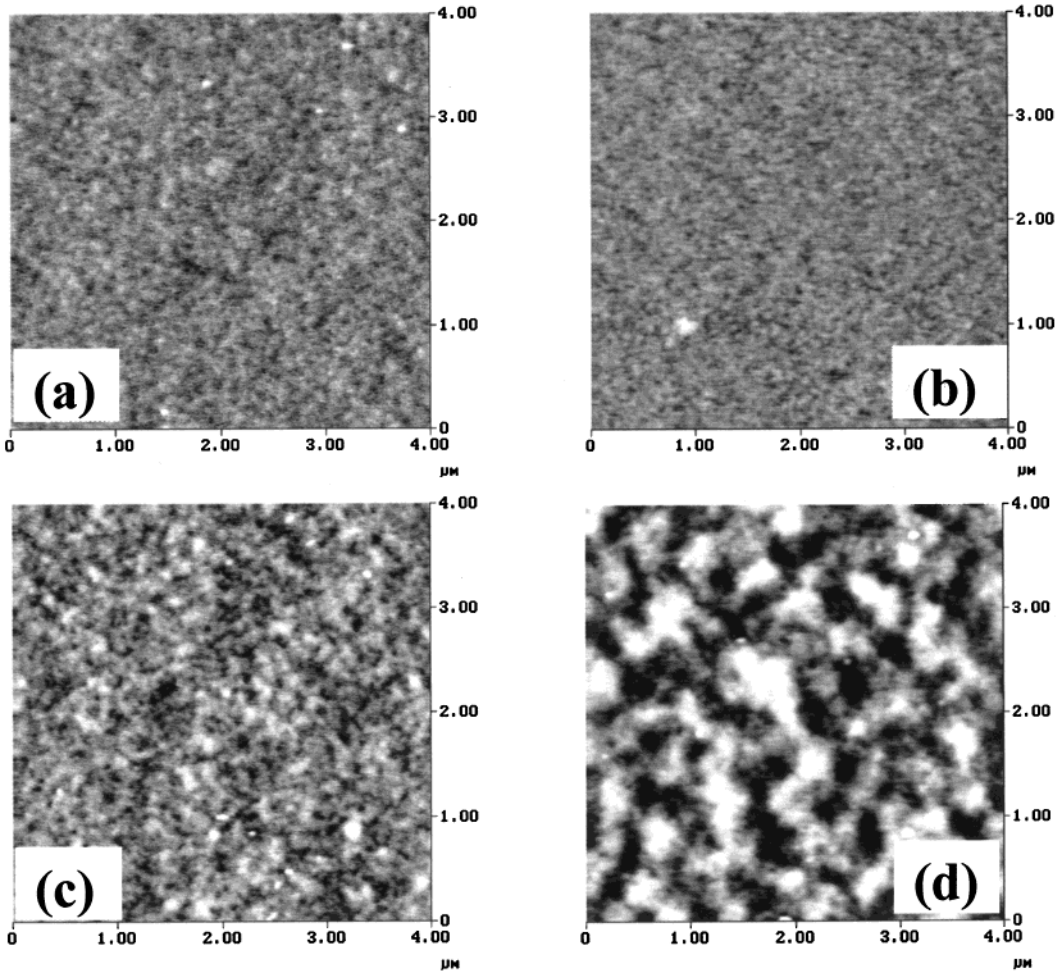

Figure 13. SPM topographical image of initial (a, b) and thermally treated (c, d) SEBS films: (a, c) grafted film 8.4 nm thick; (b, d) spin-coated film 11 nm thick. The films were heated at 150 °C for 7 h. Bright parts correspond to higher features. Vertical scale is 15 nm. "Light" tapping.

the SEBS radius of gyration (6.3 nm), we can presume that practically all chains in this film are in the contact with the surface that restrains, to some extent, in-plane expansion.

Finally, we tested thermal stability of grafted films at high temperature. The grafted film with $t = 8.4$ nm was annealed for 7 h in a vacuum oven at 150 °C. After cooling, the PS microdomain structure is completely restored, since we clearly observed the PS microdomain structure for the annealed film (Figure 11f). We compared the topography of the annealed grafted film and the film ($t = 11$ nm) spin-coated on bare silicon after an identical treatment (150 °C, 7 h). The roughness of the grafted film slightly increased from 0.3 to 0.45 nm (Figure 13a,c). On the other hand, the spin-coated film showed significant surface corrugations. Highly heterogeneous surface morphology with large corrugations was developed with microroughness increasing to 1 nm (Figure 13b,d).

Conclusions

We fabricated robust ultrathin SEBS films by melt/solution grafting to a chemically reactive silicon surface with epoxy-terminated SAM used to functionalize silicon surface. We varied the thickness of grafted block polymer, t, from 1.35 to 9.1 nm to test the limits of stability of microphase-separated structures under confined conditions. The combination of the grafting from the melt and solution allowed to vary film thickness in a wide range of t/d from 0.05 to 0.33, where d is the interdomain spacing, $d = 28$ nm, for our SEBS polymer. The contact angle measurement revealed that the surface of the block copolymer film was completely occupied by PEB chains, except the layer with the lowest thickness.

When the SEBS film reached 8.4 nm ($t/d = 0.3$), the film possessed the microdomain structure, where the PS phase forms the network cross-linking the elastomeric part. The microphase separation was completely suppressed only for films with $t/d < 0.08$. We found that, at the temperature well above T_g, PS chains were still segregated into the microdomain network. The microdomain structure became undetectable at temperatures close to the expected order−disorder transition ($T > 110$ °C). Tethered block copolymer monolayers were extremely stable at elevated temperatures unlike conventional SEBS films with comparable thickness, which had a tendency to surface corrugation and reconstruction during thermal treatment.

Acknowledgment. This work is supported by The National Science Foundation, Grant CMS-9996445. The authors thank Dr. V. V. Gorbunov for helpful discussion, P. D. Bloom and E. C. Hagberg for GPC measurements, and Shell Chemical Co. for donating SEBS sample.

References and Notes

(1) McCrum, N. G.; Buckley, C. P.; Bucknall, C. B. *Principles of Polymer Engineering*; Oxford University Press: Oxford, 1997.
(2) Huang, E.; Russell, T. P.; Harrison, C.; Chaikin, P. M.; Register, R. A.; Hawker, C. J.; Mays, J. *Macromolecules* **1998**, *31*, 7641. Harrison, C.; Park, M.; Chaikin, P.; Register, R. A.; Adamson, D. A.; Yao, N. *Macromolecules* **1998**, *31*, 2185.
(3) Mansky, P.; Russell, T. P.; Hawker, C. J.; Pitsikalis, M.; Mays, J. *Macromolecules* **1997**, *30*, 6810. Russell, T. P.; Menelle, A.; Anastasiadis, S. H.; Satija, S. K.; Majkrzak, C. F. *Macromolecules* **1991**, *24*, 6263. Walton, D. G.; Kellogg, G. J.; Mayes, A. M.; Lambooy, P.; Russell, T. P. *Macromolecules* **1994**, *27*, 6225. Kellogg, G. J.; Walton, D. G.; Mayes, A. M.; Lambooy, P.; Russell, T. P.; Galagher, P. D.; Satija, S. K. *Phys. Rev. Lett.* **1996**, *76*, 2503. Mansky, P.; Russell, T. P. *Macromolecules* **1995**, *28*, 8092.
(4) Liu, Y.; Rafailovich, M. H.; Sokolov, J.; Schwarz, S. A.; Bahal, S. *Macromolecules* **1996**, *29*, 899.
(5) Meiners, J. C.; Quintel-Ritzi, A.; Mlynek, J.; Elbs, H.; Krausch, G. *Macromolecules* **1997**, *30*, 4945.
(6) Van Dijk, M. A.; van den Berg, R. *Macromolecules* **1995**, *28*, 6773.
(7) Magonov, S. N.; Cleveland, J.; Elings, V.; Denley, D.; Whangbo, M.-H. *Surf. Sci.* **1997**, *389*, 201.
(8) Kim, G.; Libera, M. *Macromolecules* **1998**, *31*, 1, 2569.
(9) Motomatsu, M.; Mizutani, W.; Tokumoto, H. *Polymer* **1997**, *38*, 1779.
(10) Foster, M. D.; Sikka, M.; Singh, N.; Bates, F. C.; Satija, S. K.; Majkrzak, C. F. *J. Chem. Phys.* **1992**, *96*, 8605.
(11) Koneripalli, N.; Singh, N.; Levicky, R.; Bates, F. C.; Gallagher, P. D.; Satija, S. K. *Macromolecules* **1995**, *28*, 2897.
(12) Xie, R.; Karim, A.; Douglas, J. F.; Han, C. C.; Weiss, R. A. *Phys. Rev. Lett.* **1998**, *81*, 1251. Liu, Y.; Rafailovich, M. H.; Sokolov, J.; Schwarz, S. A.; Zhong, X.; Eisenberg, A.; Kramer, E. J.; Sauer, B. B.; Satija, S. *Phys. Rev. Lett.* **1994**, *73*, 440.
(13) Fasolka, M. J.; Harris, D. J.; Mayes, A. M.; Yoon, M.; Mochrie, S. G. J. *Phys. Rev. Lett.* **1997**, *79*, 3018.
(14) Russell, T. P.; Mayes, A. M.; Bassereau, P. *Physica A* **1993**, *200*, 713.
(15) Harrison, C.; Chaikin, P. M.; Huse, D. A.; Register, R. A.; Adamson, D. H.; Daniel, A.; Huang, E.; Mansky, P.; Russell, T. P.; Hawker, C. J.; Egolf, D. A.; Melnikov, I. V.; Bodenschatz, E. *Macromolecules* **2000**, *33*, 857.
(16) Mansky, P.; Chaikin, P.; Thomas, E. L. *J. Mater. Sci.* **1995**, *30*, 1987. Radzilowski, L. H.; Carvalho, B. L.; Thomas, E. L. *J. Polym. Sci., Part B* **1996**.
(17) Holden, G.; Legge, N. R. In *Thermoplastic Elastomers—a Comperhensive Review*; Holden, G., Legge, N. R., Schroeder, H. E., Eds.; Hanser: Munich, 1987; Chapter 3.
(18) Yerushalmi-Rozen, R.; Klein, J.; Fetters, L. J. *Science* **1994**, *263*, 793. Karim, A.; Tsukruk, V. V.; Douglas, J. F.; Satija, S. K.; Fetters, L. J.; Reneker, D. H.; Foster, M. D. *J. Phys. II* **1995**, *5*, 1441.
(19) Henn, G.; Bucknall, D. G.; Stamm, M.; Vanhoorne, P.; Jerome, R. *Macromolecules* **1996**, *29*, 4305.
(20) Tsukruk, V. V.; Luzinov, I.; Julthongpiput, D. *Langmuir* **1999**, *15*, 3029.
(21) Luzinov, I.; Julthongpiput, D.; Liebmann-Vinson, A.; Cregger, T.; Foster, M. D.; Tsukruk, V. V. *Langmuir* **2000**, *16*, 504.
(22) May, C. A., Ed. *Epoxy Resins: Chemistry and Technology*; M. Dekker: New York, 1988.
(23) Van Krevelen, D. W. *Properties of Polymers*; Elsevier: Amsterdam, 1997.
(24) Tsukruk, V. V. *Rubber Chem. Technol.* **1997**, *70*, 430. Tsukruk, V. V.; Reneker, D. H. *Polymer* **1995**, *36*, 1791.
(25) Ratner, B., Tsukruk, V. V., Eds. *Scanning Probe Microscopy of Polymers; ACS Symp. Ser.* **1998**, *694*.
(26) Bar, G.; Thomann, Y.; Brandsch, R.; Cantow, H.-J.; Whangbo, M.-H. *Langmuir* **1997**, *13*, 3807.
(27) Helfand, E.; Wasserman, Z. R. *Macromolecules* **1976**, *9*, 879. Helfand, E.; Wasserman, Z. R. *Macromolecules* **1978**, *11*, 960.
(28) Luzinov, I.; Minko, S.; Senkovsky, V.; Voronov, A.; Hild, S.; Marti, O.; Wilke, W. *Macromolecules* **1998**, *31*, 3945.
(29) Price, G. J.; Clifton, A. A.; Keen, F. *Polymer* **1996**, *37*, 5825.
(30) Hasegawa, H.; Hashimoto, H. *Polymer* **1992**, *33*, 475.
(31) Chen, J. T.; Thomas, E. L. *J. Mater. Sci.* **1996**, *31*, 2531.
(32) Pickering, J. P.; Vancso, G. J. *Polym. Bull.* **1998**, *40*, 549.
(33) Stapff, I.; Weidemann, G.; Shellenberg, C.; Rogenbreht, M.; Akari, S.; Antonietty, M. *Surf. Interface Anal.* **1999**, *27*, 392.
(34) Kühle, A.; Sørensen, H.; Bohr, J. *J. Appl. Phys.* **1997**, *81*, 6552.
(35) Anczykowski, B.; Krüger, D.; Babcock, K. L.; Fuchs, H. *Ultramicroscopy* **1996**, *66*, 251. Krüger, D.; Anczykowski, B.; Fuchs, H. *Ann. Phys.* **1997**, *6*, 341.
(36) Spatz, J. P.; Sheiko, S.; Möler, M.; Winkler, R. G.; Reineker, P.; Marti, O. *Nanotechnology* **1995**, *6*, 40. Spatz, J. P.; Sheiko, S.; Möler, M.; Winkler, R. G.; Reineker, P.; Marti, O. *Langmuir* **1997**, *13*, 4699.
(37) Bar, G.; Thomann, Y.; Whangbo, M.-H. *Langmuir* **1998**, *14*, 1219.
(38) Tanaka, K.; Takahara, A.; Kajiyama, T. *Macromolecules* **1997**, *30*, 6626.
(39) Jackson, C. L.; Barnes, K. A.; Morrison, F. A.; Mays, J. W.; Nakatanim, A. I.; Han, C. C. *Macromolecules* **1995**, *28*, 513.
MA000523R